Supplementary Material

Cardiomyocyte isolation and handling.

After isolation, cells were stored briefly in a high K^+ solution (in mM: 120 Glutamate [K^+ salt], 25 KCl, 1 $MgCl_2$, 10 HEPES, 1 EGTA, pH 7.2 with KOH) and either used immediately or transferred to Dulbecco's Modification of Eagle's Medium (10-013 DMEM, Mediatech, Inc. Virginia) in laminin-coated petri dishes in a 95% O_2, 5% CO_2 incubator at 37°C for at least 2 h before imaging. As previously described (1), experimental recordings started after exchange of the DMEM with an experimental Tyrode's solution containing (in mM): 140 NaCl, 5 KCl, 1 $MgCl_2$, 10 HEPES, 1 $CaCl_2$, pH 7.4 (adjusted with NaOH), supplemented with 10 mM glucose. The dish containing the cardiomyocytes was equilibrated at 37°C with unrestricted access to atmospheric oxygen on the stage of a Nikon E600FN upright microscope.

Additional controls

In order to investigate whether the excitation wavelength, λ_{exc}, and laser intensity affected the results obtained with RDA or PSA, TMRM-loaded cardiomyocytes were subjected to the imaging conditions described under M&M at λ_{exc} = 740 nm or λ_{exc} = 800 nm at several different laser intensities. Similar results were obtained under all conditions tested. More importantly, to account for the instrument response of the detectors, we compared the time evolution of the mitochondrial TMRM fluorescence with the background signals recorded in the same stack of images. Unlike the high correlation detected by either RDA or PSA in the time series, the background showed behavior similar to white noise with $D_f \approx 1.5$ or $\beta \approx 0.0$, for RDA or PSA, respectively. Additional control recordings were also made using fluorescently-labeled beads imaged under the same conditions, which yielded spectra that did not show scale invariant properties (data not shown).

Nearest neighbors exhibit temporal correlation in spatially heterogeneous systems.

The correlation between nearest neighbors in a spatially heterogeneous system (e.g. the mitochondrial network of heart cells) can be expressed in terms of covariance between pairs of observations of a certain variable ($\Delta\Psi_m$) through the spatial correlation coefficient, r_1, (2):

$$r_1 = 2^{3 - 2D} - 1 \qquad [1]$$

The key to the derivation of this expression is, first, that the correlation is expressed via the covariance between pairs of observations and, second, that the relative dispersion or coefficient of variation, CV, of aggregates of nearest neighbors obey a fractal relationship (3). Equation [1] can also be applied to fractal random time series as those analyzed in the present work, in addition to spatially inhomogeneous data sets, where D (D_f in our work) is the fractal dimension in either case (4) (see also legend Fig. S1). The derivation of the single-time-lag correlation coefficient, r_1, of a time series (4) is based on similar arguments as those used for Eq. [1] (2, 3).

If there is no temporal correlation, r_1=0, then the behavior of mitochondria is completely random and D_f=1.5, as expected from white noise type of behavior. With perfect correlation, r_1=1, the mitochondrial behavior is correlated everywhere (3). When the D_f obtained from RDA analysis (Fig. 3; see also the main text) was substituted into

eq. [1] we obtained temporal correlations, r_1, within the range 0.96-0.98 ($D_f \approx 1.01$) for the "physiological domain" and around 0.80 ($D_f \approx 1.08$) for the "pathophysiological domain" (Fig. S1). Interestingly, we have previously shown that ~80% of the mitochondrial network behaved synchronously under pathophysiological conditions using grid analysis of TMRE time series (1), suggesting that the network is correlated in both time and space.

Lognormal and power law distributions.

Lognormal and 1/*f* distributions may be confused; thus, we performed a series of tests to see whether our power spectra behaved according to inverse power laws (Fig. S2). The lognormal distribution is the familiar normal distribution but in the logarithm of a given variable, e.g. fluorescence intensity. On a log-log plot an inverse power law graphs as a straight line. The underlying basis of a lognormal distribution is a multiplicative relationship of interdependent events. The distribution of lognormal systems becomes broader as they turn more complex and start to resemble a 1/*f*-distribution characterized by an inverse power law. In our data, this happens at the 80th percentile (Fig. S2B) where the distribution deviates sharply from lognormal. In general, the size of the interval over which the 1/*f* and lognormal distributions coincide increases as the width of the lognormal distribution increases. Otherwise stated, if the lognormal distribution has a large variance, corresponding to a process comprised of a large number of subtasks, and we sample the process in the region of large *f*, then we would be unable to distinguish between the lognormal and 1/*f*-distributions (4).

Pink noise

Pink noise was calculated according to D. J. Hermes and M. Schram (2004) (Eindhoven University of Technology, The Netherlands) (Fig. S3). Similar analyses rendering the expected results were applied to white noise obtained from random shuffling of correlated time series (Fig. 4B) or the instrument noise of the background (Fig. 3D). The best result of the expected β for pink noise was achieved with the rectangular windowing method of the FFT algorithm used to perform the calculations (Fig. S3) (Microcal Origin$_{TM}$, Northampton, MA) (see also M&M: *FFT calculation*).

Simulation of brown noise

The position of a Brownian particle as a random function of time simulates brown noise. The increments in the position of the Brownian particle are given by (5): $X(t) - X(t_0) \sim \xi \left|t - t_0\right|^H \quad (t > t_0)$, for any two times t and t_0 with H=0.5 for ordinary Brownian motion. With this equation one obtains the time series shown in Fig. 3E as represented by the position X(t) given $X(t_0)$ by choosing a random number from a Gaussian distribution, multiplying it by the time increment $\left|t - t_0\right|^H$ and adding the result to the given position $X(t_0)$.

A theoretical simulation of the inverse power law behavior exhibited by the mitochondrial network of cardiomyocytes

Self-sustained and highly coordinated oscillations in $\Delta\Psi_m$, ROS, NADH and reduced glutathione can be triggered under conditions of oxidative stress (Aon et al.,

2003), which could be reproduced in a computational model of ROS-induced ROS release. The model represents mitochondrial energetics (6) coupled to ROS production, transport and scavenging (7). Mathematically, the model is described by a system of 15 ordinary differential equations (ODEs) that under appropriate conditions is able to exhibit Hopf bifurcations, a signature of the presence of stable limit-cycle (oscillatory) dynamics (7). A striking property of the mitochondrial oscillator model is its capacity to modulate the oscillatory period for a wide temporal range spanning from milliseconds to hours. This modulation occurs within the oscillatory domain after a Hopf bifurcation, in response to one parameter that affects the rate of ROS scavenging by superoxide dismutase (7).

According to the model, the double log plot of amplitude *versus* frequency exhibits an inverse relationship (Fig. 7A). This relationship is mechanistically at the origin of the inverse power law behavior (see the main text section: *Origins of the inverse power law behavior*).

The simulations shown in Figure S4 demonstrate that the lower the period, the higher the amplitude. It can also be seen that $\Delta\Psi m$ deflections of 30mV up to a few μV are within the high frequency low amplitude range of behavior that we attribute to the physiological domain (Fig. S4B). From the simulations, we selected five oscillatory periods in the high frequency domain (between 70 and 300ms) and one from the low frequency (1 min period) domain and attributed each one of them proportionally to a network composed by 500 mitochondria (i.e. every 100 mitochondria will oscillate with the same period). This number of mitochondria is similar to that present in a single optical slice of a cardiomyocyte (~ 1μm focal depth) that we analyze by two-photon laser scanning microscopy with 110ms/frame time resolution. Our experimental results could be simulated with a mixture of 80% short period and 20% long-period oscillations.
According to this protocol, we then constructed a matrix:

	Mito 1	**Mito 2**	**Mito 3**	... Mito n
T_0				
T_1				
T_2				
$\ldots T_n$				

with mitochondria in columns and time, T_i, on rows. The final matrix contained a total of 500 columns and 6,000 rows. The time steps represented by the rows correspond to a fixed integration step of 20ms for the numerical integration of the system of ODEs. The fixed integration step of 20ms was kept for the simulation of all periods within the range of 70 to 300ms and 1 min period.

The average value of each row of the matrix at e.g. time 1, T_1, represents the experimental average value of fluorescence intensity of the ΔΨm probe (corresponding to mV) obtained every 110ms from 500 mitochondria (on average) from each image of our stack. Thus, by applying this procedure to the whole matrix we obtain a column of average values of millivolts that is the analog of the ΔΨm fluorescent probe time series obtained in our experiments. By applying RDA and PSA (see M&M of our manuscript) to the theoretical time series obtain a result that resembles the experimental results as shown in Fig. S5. More specifically, we reproduce the spectral exponent, β, obtained from PSA (Fig. S5B, left panel) and the fractal dimension, D_f, calculated from RDA (Fig. S5B, right panel). Included at the top right panel of Fig. S5 is a plot of random behavior (in red) for comparison.

Theoretical simulation of the decrease in β observed experimentally in the presence of respiratory or inner membrane anion channels inhibitors.

From inspection of Figure 5 of the manuscript we can see that the major impact of both inhibitors is in the high frequency, low amplitude region of the power spectrum. Since these inhibitors decrease ROS production or transport to the cytoplasm either by blocking respiration, or by inhibiting ROS-induced ROS release from mitochondria, respectively, and ROS is the chemical messenger involved in mitochondrial coupling, we hypothesized that a decrease in coupling will result in an increase of mitochondrial random dynamics.

Random dynamics in our computational model were simulated by randomizing oscillatory time series mixing them equally among the different oscillatory periods described above. Thus, a 20% randomization corresponds to a total of 20 mitochondria out of every 100 behaving randomly in each of the five frequency bands. As proven by PSA, randomization appears as white noise (Fig. 6E of the manuscript). Experimental evidence for increased random behavior is given by the analysis of mitochondria outside the synchronized oscillating mitochondrial cluster in the pathophysiological regime (compare panels C and D in Fig. 6 of the manuscript). The results obtained are shown in Fig. S6. We can clearly see a decrease in β with 20% (Fig. S6B) and 40% (Fig. S6C) randomization with respect to the control (Fig. S6A) either in the power spectrum (Fig. S6B and S6C, left panels) or in the high frequency domain (Fig. S6B and S6C, right panels). As expected, the major effect is in the high frequency low amplitude region of the power spectrum (compare right panels of Fig. S6A-C).

Simulating the transition between physiological and pathophysiological domains of behavior of the mitochondrial network.

By adopting a similar approach as the one described above, we constructed a matrix of short period oscillations (Fig. S7B, top right panel; the inset represents a zoom of the main panel) and started to increase the proportion of the long-period 1 min oscillation (large depolarizations of ΔΨm that corresponds to pathophysiological behavior). When the latter represents 60% of the network, most the overall system dynamics are dominated by the low frequency (Fig. S7B, right bottom panel) similar to what happens experimentally and observed as a single mode lock (~ 100s in the experiments) (Fig. S7A, right panel). Both the extent of ΔΨm depolarization (~ 90mV) and the critical percentage of mitochondria (~ 60%) are in agreement with the

experimental data. Accordingly, the return plot of the TMRM time series could be simulated (Fig. S7B).

References

1. Aon, M. A., S. Cortassa, E. Marban, and B. O'Rourke. 2003. Synchronized whole cell oscillations in mitochondrial metabolism triggered by a local release of reactive oxygen species in cardiac myocytes. J Biol Chem 278:44735-44744.
2. van Beek, J. H. G. M., S. A. Roger, and J. B. Bassingthwaighte. 1989. Regional myocardial flow heterogeneity explained with fractal networks. Am. J. Physiol. 257:H1670-H1680.
3. Bassingthwaighte, J. B., L. S. Liebovitch, and B. J. West. 1994. Fractal Physiology. Oxford University Press, New York.
4. West, B. J. 1999. Physiology, promiscuity and prophecy at The Millennium: A tale of tails. World Scientific, Singapore.
5. Feder, J. 1988. Fractals. Plenum Press, New York.
6. Cortassa, S., M. A. Aon, E. Marban, R. L. Winslow, and B. O'Rourke. 2003. An integrated model of cardiac mitochondrial energy metabolism and calcium dynamics. Biophys J 84:2734-2755.
7. Cortassa, S., M. A. Aon, R. L. Winslow, and B. O'Rourke. 2004. A mitochondrial oscillator dependent on reactive oxygen species. Biophys J 87:2060-2073.
8. Aon, M. A., S. Cortassa, and B. O'Rourke. 2004a. Percolation and criticality in a mitochondrial network. Proc Natl Acad Sci U S A 101:4447-4452.

Figures and Video sequence legends.

Figure S1. Temporal correlation of mitochondria as a function of the fractal dimension.
The fractal dimension, D_f, obtained according to RDA (see Fig. 3 and main text) was used to calculate the single-time-lag correlation coefficient, r_1 (Eq. 1). The plot of r_1 versus D_f is shown.

Figure S2. Power law distribution of TMRM fluorescence time series obtained from heart cells.
The frequency histogram in panel A shows a long tail as a signature of an inverse power law that is also revealed by the frequency of appearance of certain fluorescence values in time as a function of their cumulative probability (panel B). In this type of graph the distribution is lognormal out to the 80th percentile, after which it deviates sharply indicating again an inverse power law. The log-log plot displayed in panel C shows that the inverse power law graphs as a straight line.

Figure S3. Time series, RDA and PSA of pink noise.
Shown in panel A is the plot of the time series obtained with the simulation of pink noise (35,281 points). Panels B and C show the results obtained with PSA and RDA, respectively. The value of $\beta = 1.0$ is the expected one for pink noise whereas $D_f \approx 1.0$ corresponds to almost perfect correlation (see also Fig. S1).

Figure S4. Modulation of the period and amplitude of oscillations through changes in the rate of ROS scavenging by superoxide dismutase (SOD).
The simulations for shunt = 0.1 and SOD concentrations as shown in panel A were performed with the following set of parameters (see (6, 7), for detailed parameter

descriptions): concentration of respiratory chain carriers, ρ^{REN}=2.50x10^{-6} mM; concentration of F1F0 ATPase, ρ^{F1}=2.03x10^{-3} mM; $[Ca^{2+}]_i$=0.1 μM; K_{cc}=0.01 mM; k^1_{SOD} =2.4x10^6 mM^{-1}s^{-1}; k^1_{CAT} =1.7x10^4 mM^{-1}s^{-1}; G_T=0.5 mM; maximal rate of the adenine nucleotide translocase, V_{maxANT}=5 mM s^{-1}; and maximal rate of the mitochondrial Na-Ca exchanger, V_{max}^{NaCa} = 0.015 mM s^{-1}.

Figure S5. Simulation of the inverse power law behavior observed after RDA or PSA of the fluorescence time series of TMRM.

Simulations were performed as described in the Supplementary material text with model parameters mentioned in the legend of Fig. S4. The matrix was constructed as described in this supplement under the section: *A theoretical simulation of the inverse power law….*

Figure S6. Simulation of the effect of inhibitors on the spectral exponent, β, of the high frequency domain of the power spectrum.

The simulation of oscillatory behavior and the matrix construction were performed as described in the legend of Figs. S4 and S5, and in the text of this supplement. The percentage of randomized time series was gradually increased and equally distributed in all frequencies. The results obtained with 20% and 40% of randomization (panels B and C) are shown in comparison with the control (panel A). The panels on the right show that the decrease in β is mainly due to the effect of randomization on the high frequency domain of the spectrum.

Figure S7. Simulation of the transition between physiological and pathophysiological regimes.

The percentage of low period (1 min) oscillations that correspond to high amplitude $\Delta\Psi_m$ depolarization was gradually and proportionally increased in the matrix of 500 oscillators. Panel B, right top, corresponds to the initial mixture of five different high frequencies (within the range of 75ms to 300ms) while the right bottom panel described the mixture of those five frequencies but with a 60% of the low frequency that dominates the dynamic output of the system, i.e. the large amplitude $\Delta\Psi_m$ depolarization. The 60% of the mitochondrial network showing 1 min oscillations with 80mV amplitude is in agreement with experimental observations (1, 8).

Video of a cardiomyocyte loaded with TMRM that shows the physiological and pathophysiological regimes of the mitochondrial network dynamic behavior. This video collected from two-photon scanning laser microscopy at 150ms/frame corresponds to a stack of 3,720 images whose temporal sequence is shown in Fig. 1 of the main text. The sequence is shown compressed at 70frames/second.

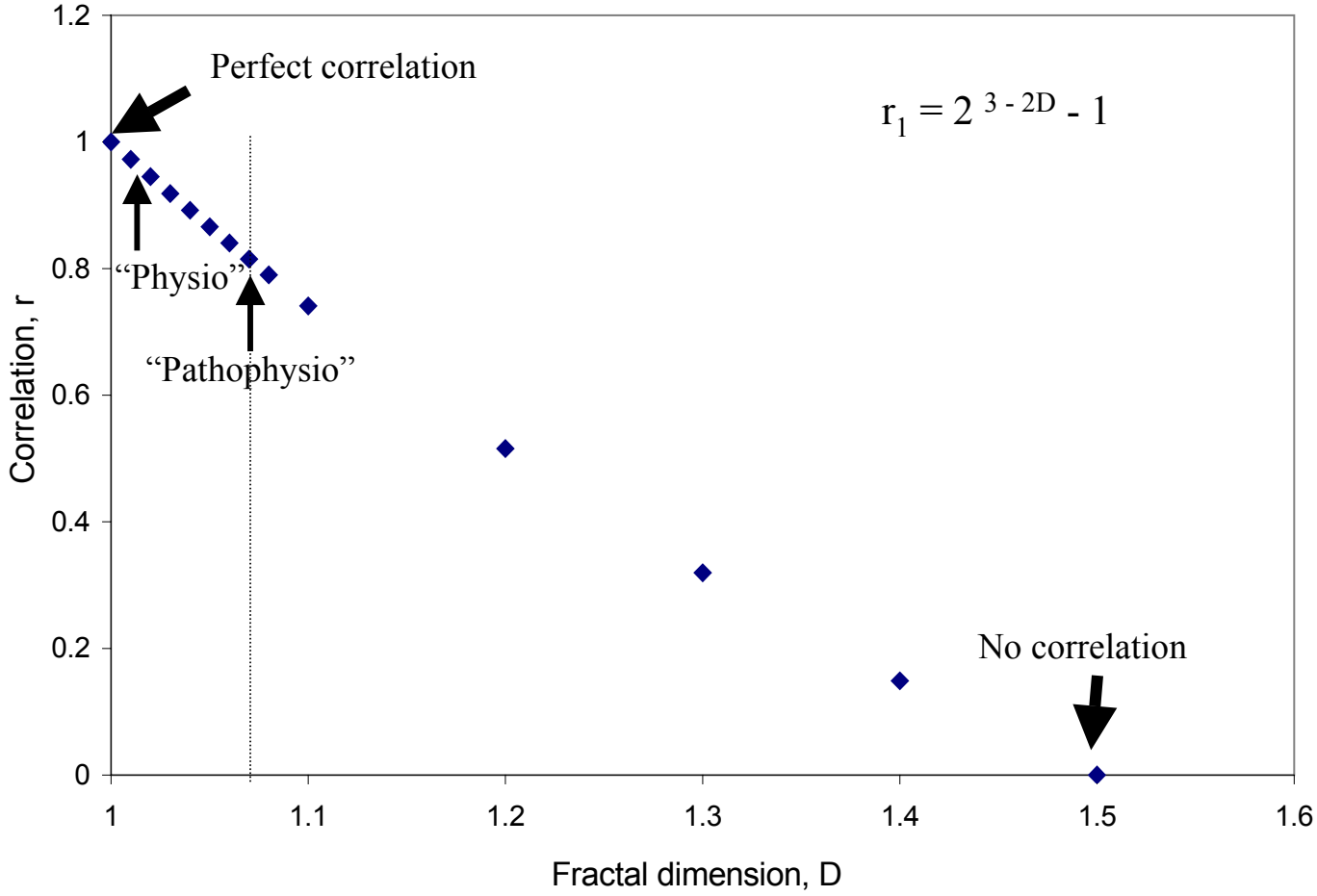

Figure S1. Aon, Cortassa, O'Rourke. 2006

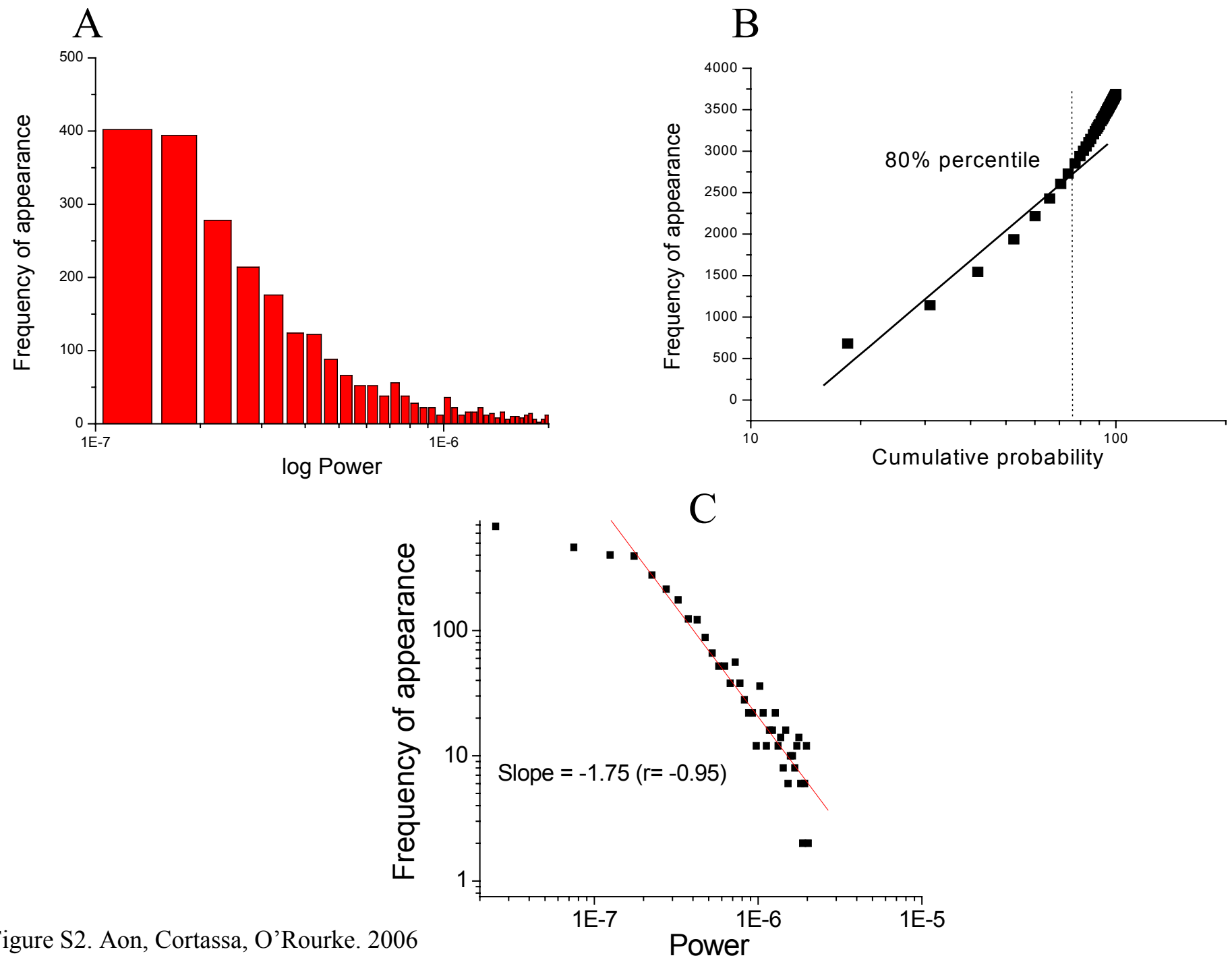

Figure S2. Aon, Cortassa, O'Rourke. 2006

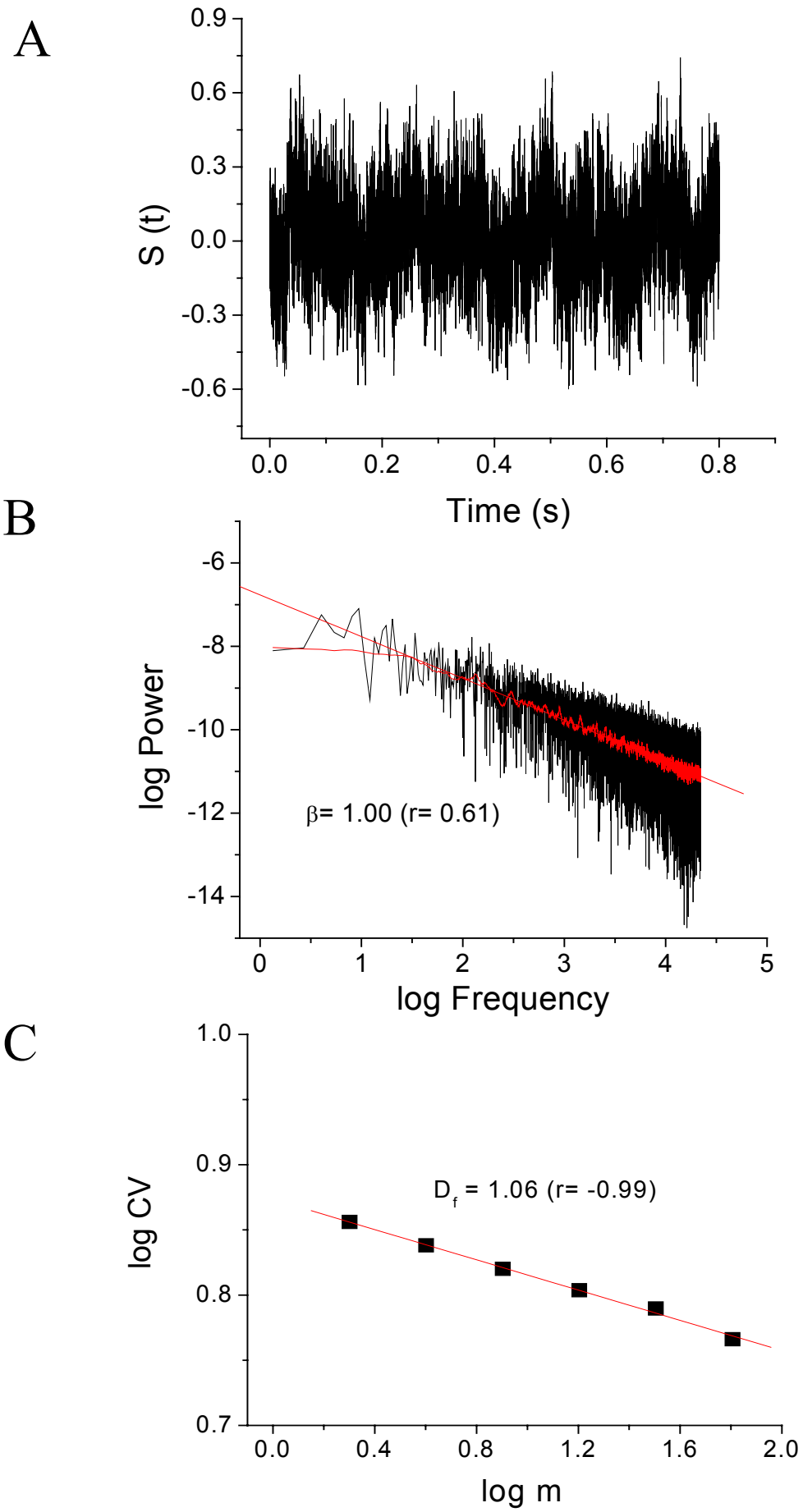

Figure S3. Aon, Cortassa, O'Rourke. 2006

PERIOD MODULATION OF THE MITOCHONDRIAL OSCILLATOR IN THE HIGH FREQUENCY DOMAIN

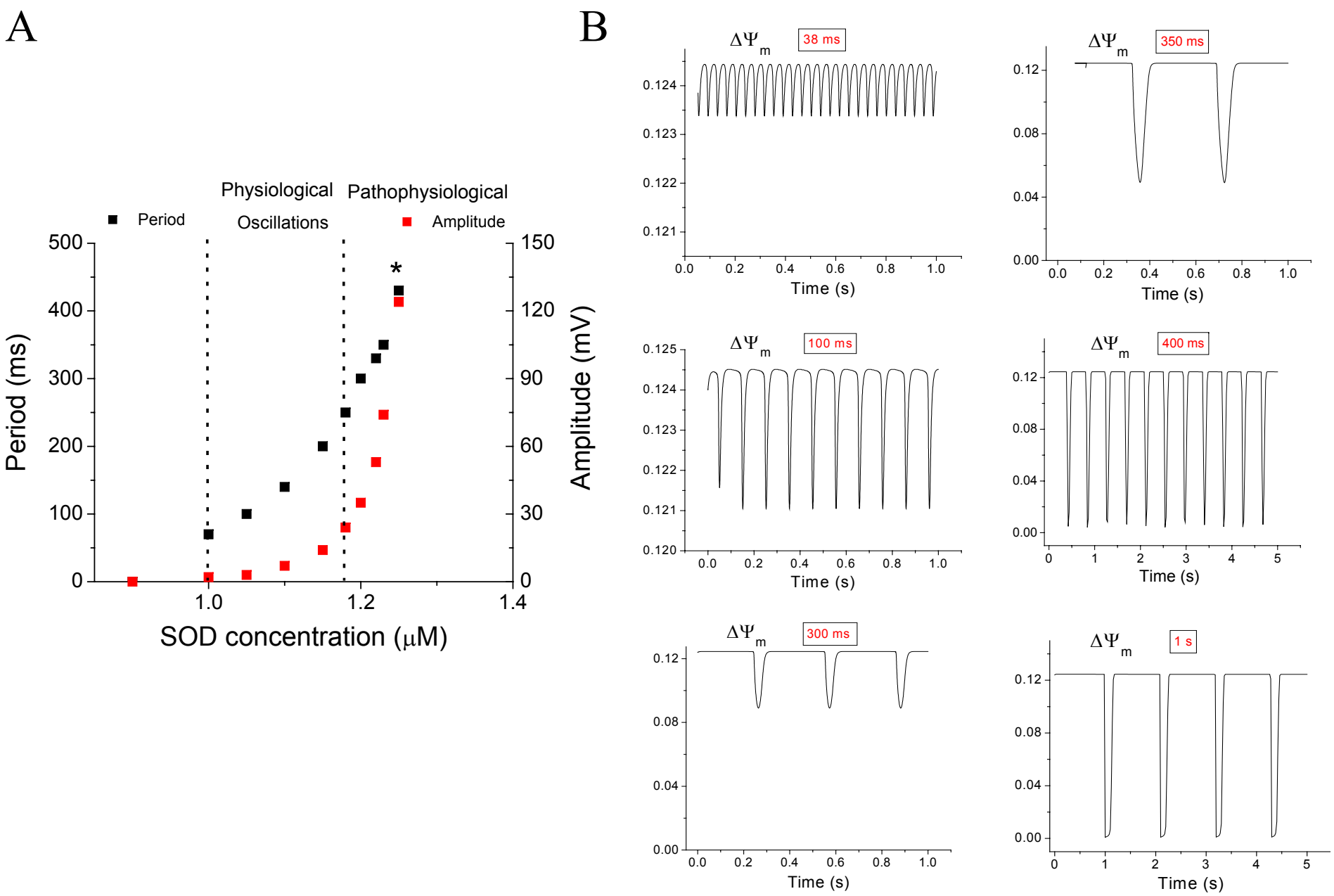

Figure S4. Aon, Cortassa, O'Rourke. 2006

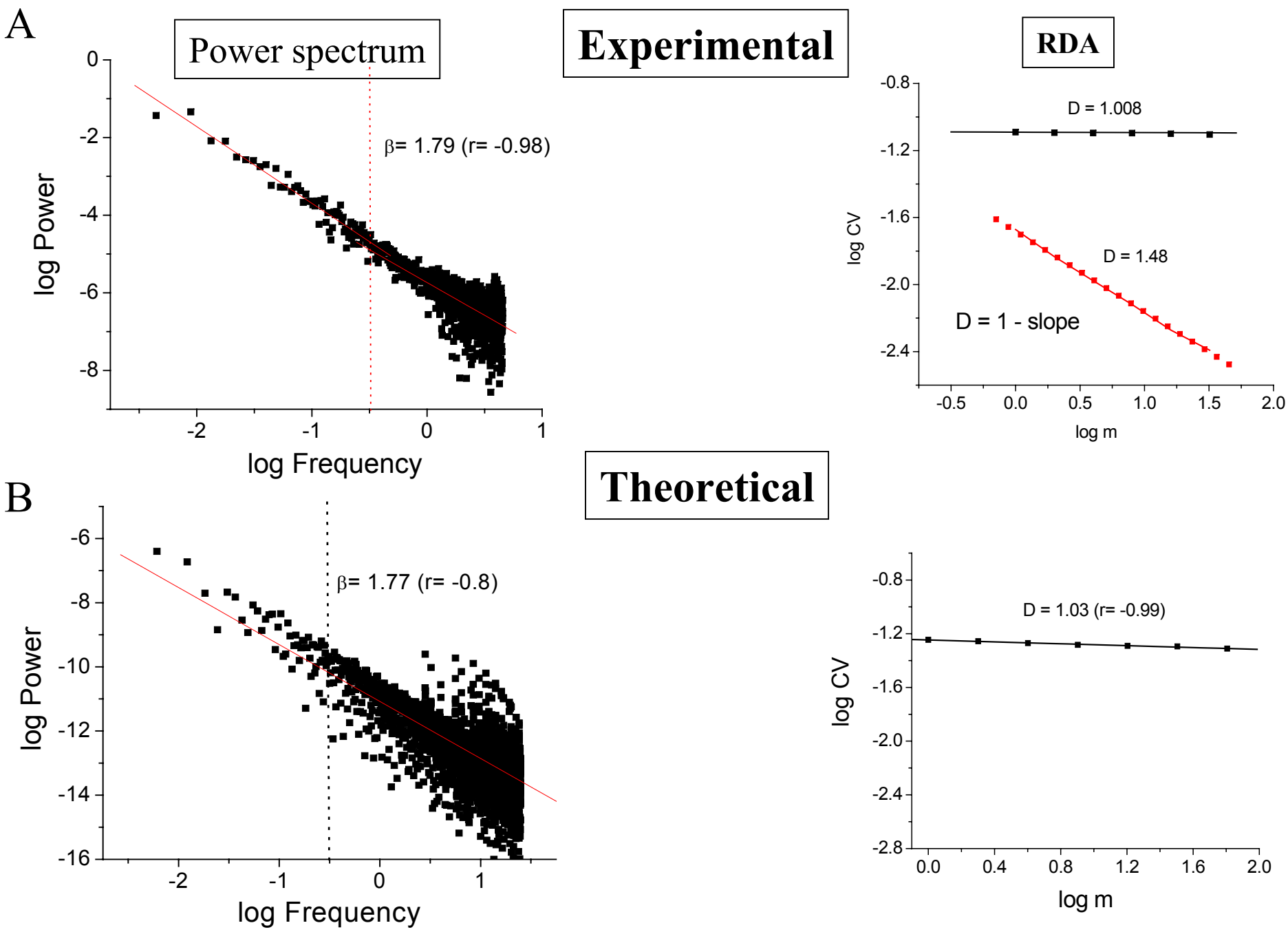

Figure S5. Aon, Cortassa, O'Rourke. 2006

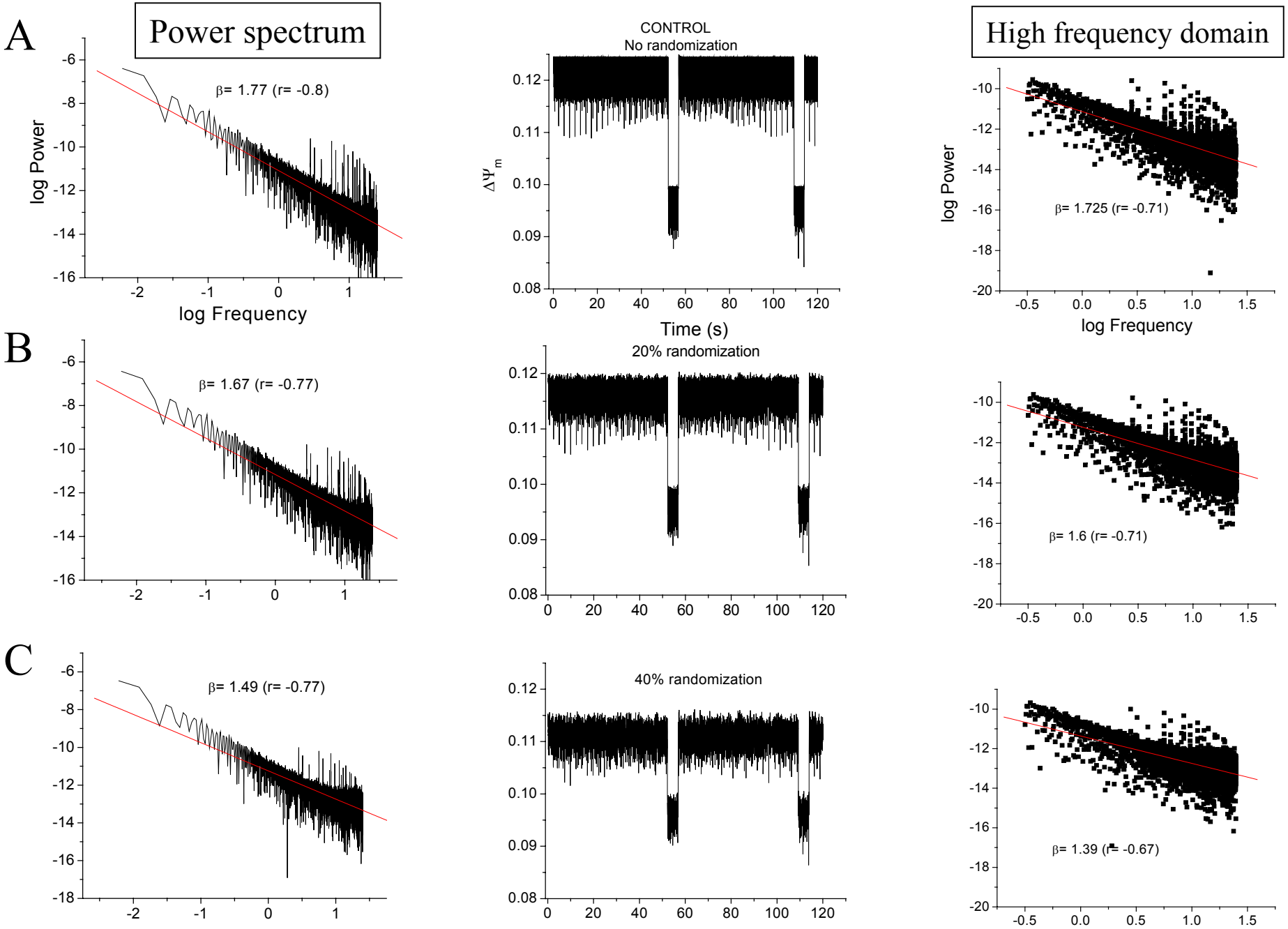

Figure S6. Aon, Cortassa, O'Rourke. 2006

EXPERIMENTAL

A

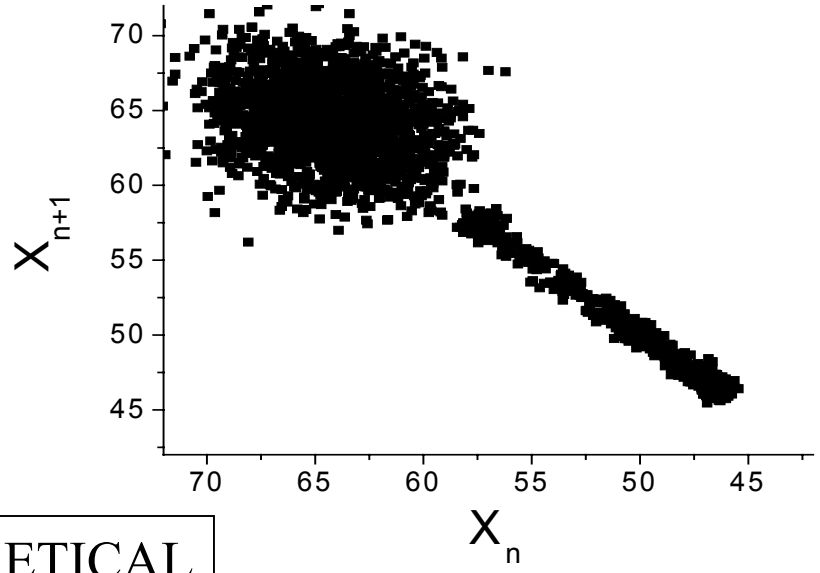

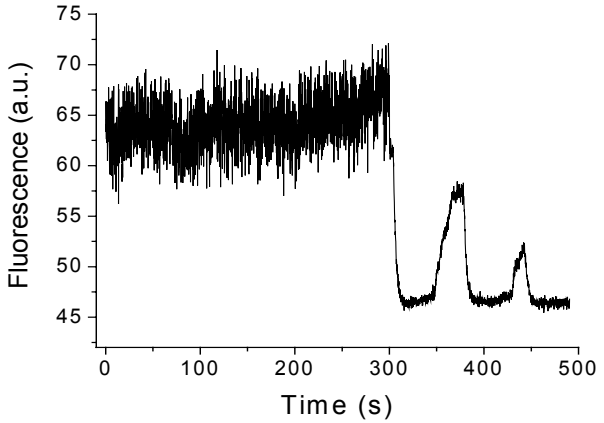

THEORETICAL

B

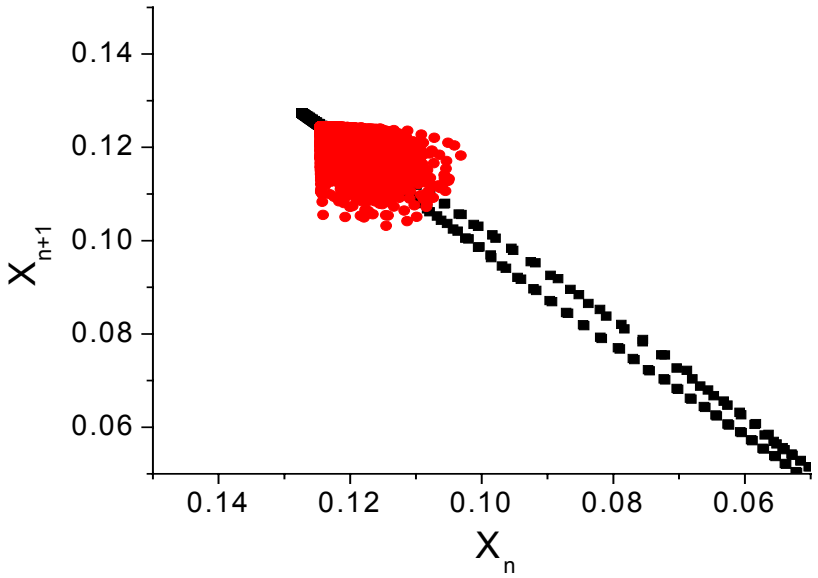

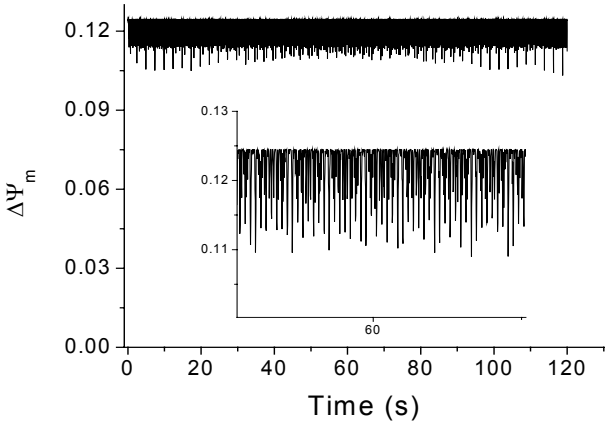

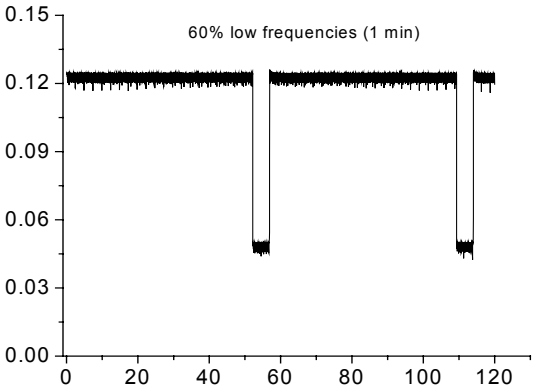

Figure S7. Aon, Cortassa, O'Rourke. 2006